Nuclear Materials and Energy 19 (2019) 149–154

Contents lists available at ScienceDirect

Nuclear Materials and Energy

journal homepage: www.elsevier.com/locate/nme

Characteristics of plasma flow profiles in a super-X-divertor-like configuration

Satoshi Togo[*,a,1], Tomonori Takizuka[b], Dirk Reiser[c], Mizuki Sakamoto[a], Yuichi Ogawa[d], Naomichi Ezumi[a], Kenzo Ibano[b], Kunpei Nojiri[a], Yue Li[d], Yousuke Nakashima[a]

[a] Plasma Research Center, University of Tsukuba, 1-1-1 Tennodai, Tsukuba, 305-8577, Japan
[b] Graduate School of Engineering, Osaka University, 1-1 Yamadaoka, Suita, 565-0871, Japan
[c] Forschungszentrum Jülich GmbH, IEK-Plasmaphysik, Jülich, 52425, Germany
[d] Graduate School of Frontier Sciences, University of Tokyo, 5-1-5 Kashiwanoha, Kashiwa, 277-8568, Japan

ARTICLE INFO

Keywords:
Super-X divertor
Plasma fluid model
Anisotropic ion pressure
Magnetic nozzle effect
Supersonic plasma flows
Bohm criterion

ABSTRACT

Plasma flow patterns in a super-X-divertor-like configuration are investigated by using a one-dimensional plasma fluid model with the anisotropic-ion pressure (AIP model). The AIP model enables to treat supersonic plasma flows self-consistently by describing the parallel plasma momentum transport with a hyperbolic equation keeping the finite effect of the parallel viscosity. A supersonic plasma flow in the diverging-magnetic-field divertor region is generated due to the magnetic nozzle effect. It is found that the sonic-transition point has bifurcation characteristics. A numerical solution from the AIP model agrees well with an analytical one. The Braginskii's plasma fluid model, on the other hand, creates various unphysical profiles in the supersonic plasma flow region for different boundary conditions of the plasma flow at the sheath entrance. It is also found that a particle source/sink in front of the target brings about generations of subsonic/supersonic plasma flow profiles. Moving the target position, it is found that a discontinuous change in the sonic-transition point and corresponding profile of plasma flow can happen due to the bifurcating characteristics of the sonic-transition point.

1. Introduction

Handling of the particle and heat loads onto the divertor plates is one of the most crucial issues in future fusion devices. Various concepts of novel divertors such as a super-X divertor (SXD) [1] and a snowflake divertor [2] have been proposed for DEMO reactors in order to resolve this issue. In an SXD, the position of the outer divertor plate in major radius is further compared to an ordinary divertor which brings about an increased total flux expansion and an increased plasma-wetted area. Thus, it is expected that the particle and heat loads onto the outer divertor plate can be efficiently reduced in an SXD. In a realistic situation, however, moving the outer divertor plate in major radius simultaneously changes other characteristics of the divertor plasma including radial transport of plasma particles and heat, neutral confinement and efficiency of impurity radiation. The performance of an SXD, therefore, has been researched from experimental [3–5], numerical [6–8] and theoretical [9–11] points of view.

The scrape-off layer (SOL)-divertor region in a torus plasma with an SXD has a magnetic-nozzle structure caused by its enlarged total flux expansion. It has been demonstrated from theories [12,13] and experiments [14,15] that a supersonic plasma flow might be caused by the magnetic nozzle effect. A self-consistent treatment of the plasma flow can, thus, be important in theoretical and numerical studies on the performance of an SXD because a supersonic plasma flow makes the plasma density lower and affects atomic and molecular (A&M) processes and impurity radiation. In theoretical studies of an SXD, however, the sonic-transition point is designated in advance. As for numerical simulations based on a widely-used plasma fluid model (so-called the Braginskii equations [16]), an explicit boundary condition of the plasma flow velocity at a sheath entrance is required such as the Mach number of unity, which is the lower limit of the Bohm criterion, in order to solve the equation of parallel plasma momentum. It is hence difficult to self-consistently treat the plasma flow in conventional ways of theoretical and numerical studies of an SXD.

Attempts to self-consistently treat supersonic plasma flows have been made for example in Refs [17–19]. In these earlier studies, however, the equation of parallel plasma momentum is described in hyperbolic type by neglecting the parallel viscosity term and does not

* Corresponding author.
E-mail addresses: togo@prc.tsukuba.ac.jp, Satoshi.Togo@iter.org (S. Togo).
[1] Current affiliation: ITER Organization, Route de Vinon sur Verdon, 13067 St Paul Lez Durance Cedex, France

https://doi.org/10.1016/j.nme.2019.02.016
Received 14 August 2018; Accepted 11 February 2019

require an explicit downstream boundary condition. We have been developing a one-dimensional (1D) plasma fluid code, where the anisotropic ion pressure (AIP) or the anisotropic ion temperature is directly incorporated in the fluid equations [20–24]. This AIP model enables to make the equation of parallel plasma momentum hyperbolic keeping the finite effect of the parallel viscosity. A virtual divertor (VD) model is used instead of an explicit boundary condition at a sheath entrance. Supersonic plasma flows in a radiative-cooling divertor plasma [21] and in a diverging-magnetic-field divertor plasma [23] were successfully realized. In the present paper, we apply this AIP model to an SXD-like configuration and investigate characteristics of supersonic plasma flow profiles.

2. Numerical model

2.1. Plasma fluid models

In the AIP model, the parallel and perpendicular components of ion pressure, $p_{i,\parallel}$ and $p_{i,\perp}$, are directly incorporated in the plasma fluid model for inhomogeneous magnetic fields [23,24]. The equations of continuity of ions and parallel plasma momentum are shown below;

$$\frac{\partial n}{\partial t} + B\frac{\partial}{\partial s}\left(\frac{nV}{B}\right) = S, \tag{1}$$

$$\frac{\partial}{\partial t}(m_i nV) + B\frac{\partial}{\partial s}\left[\frac{1}{B}(m_i nV^2 + p_{i,\parallel} + p_e)\right] + \frac{p_{i,\perp} + p_e}{B}\frac{\partial B}{\partial s} = M_m. \tag{2}$$

Eqs. (1) and (2) are solved with those of parallel ion energy, perpendicular ion energy and (isotropic) electron energy which are shown as Eqs. (3)–(5) in Ref. [24] and omitted in this paper. Here, the pressures are defined by $p_\sigma = nT_\sigma$ in which σ stands for the species and components as $\sigma \in \{(i, \parallel), (i, \perp), i, e\}$. Note that Eq. (2) is hyperbolic. In the Braginskii equations [16], on the other hand, the equation of parallel plasma momentum is described in terms of the isotropic and anisotropic parts of ion pressure, $p_i \equiv (p_{i,\parallel} + 2p_{i,\perp})/3$ and $\delta p_i \equiv 2(p_{i,\parallel} - p_{i,\perp})/3$ as follows;

$$\frac{\partial}{\partial t}(m_i nV) + B\frac{\partial}{\partial s}\left(\frac{m_i nV^2}{B}\right) + B^{3/2}\frac{\partial}{\partial s}(B^{-3/2}\delta p_i) = -\frac{\partial}{\partial s}(p_i + p_e) + M_m, \tag{3}$$

which is mathematically equivalent to Eq. (2). The anisotropic part δp_i in Eq. (3) is approximated by a parallel viscous flux, $\delta p_i \approx -\eta_\parallel B^{-1/2}\partial_s(B^{1/2}V)$, making this equation parabolic. The B2 code [25], which is based on the Braginskii equations, is also partly used for comparisons with the AIP model. The notations of variables and the calculation conditions concerning these two models are the same as Ref. [24] except for boundary conditions of the plasma flow velocity at the sheath entrance used in the B2 code which are described in detail in Section 3.3. The plasma sound speed is defined by $c_s \equiv \sqrt{(T_{i,\parallel} + T_e)/m_i}$ in the AIP model and $c_s \equiv \sqrt{(T_i + T_e)/m_i}$ in the B2 code, respectively.

2.2. SXD-like configuration

Fig. 1(a) shows the parallel-to-**B** (the coordinate of which is denoted by s) profiles of the magnetic-field strength B and corresponding cross-sectional area of the flux tube A used in this study which is the same as Ref. [24]. The system length is $L = 2.82$ m. The particle source term is artificially given as $S = S_0 \exp[-20(s/L)^2]$ with $S_0 = 1.11 \times 10^{23}$ /m$^3\cdot$ s as shown in Fig. 1 (b). The heat source terms are given as $Q_i = Q_e = (3/2)T_{in}S$ with the source temperature $T_{in} = 10$ eV and Q_i is isotropically divided into $Q_{i,\parallel} = Q_i/3$ and $Q_{i,\perp} = 2Q_i/3$ for the AIP model. The momentum source M_m is set to be zero. As for the boundary conditions, a mirror symmetric condition (i.e. $\partial_s n = V = \partial_s T = 0$) is imposed at $s = 0$. The target is set at $s = L_t$ and $L_t = L$ for Sections 3.1–3.4. For Section 3.5, L_t is changed in the range of $L/2 \le L_t \le L$. The system has the local maximum of B at $s = 2.39$ m giving

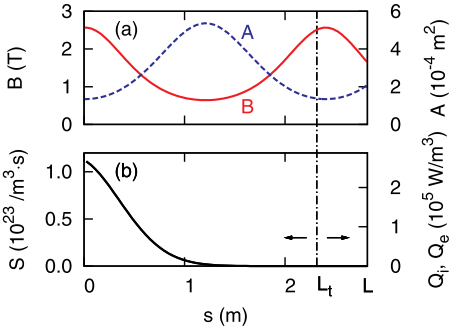

Fig. 1. Calculation conditions used in this study; parallel-to-**B** profiles of (a) the magnetic field strength B (solid line), the cross-sectional area of the flux tube A (broken line) and (b) source terms. The vertical chain line represents the target position.

a magnetic nozzle structure in front of the target except for when $L_t < 2.39$ m. The VD model [21] is used for $s > L_t$ for the sheath boundary condition at $s = L_t$ in the AIP model while the plasma flow velocity V at $s = L_t$ (denoted by V_t) is prescribed in the B2 code in Section 3.3.

3. Results and discussions

3.1. Numerical solution from the AIP model

Fig. 2 shows the numerical solution in the steady state obtained from the AIP model. As shown in Fig. 2 (b) and (d), $n \sim 5.88 \times 10^{18}$ /m^3 and $T_i \sim 5.48$ eV ($T_{i,\parallel} \sim 5.07$ eV and $T_{i,\perp} \sim 5.69$ eV) are observed at $s = 0$. The mean free path of ion-ion Coulomb collisions is thus evaluated to be m $\ll L$. That is why an almost isotropic T_i is obtained. The Mach number $M \equiv V/c_s$ is comparably low in the upstream diverging magnetic field region and starts to increase in the downstream contracting and diverging magnetic field region (i.e. a magnetic nozzle) as shown in Fig. 2 (c). By assuming that $V \approx 0$, $T_{i,\parallel} \approx T_{i,\perp}$ and $T_{i(e)} \approx$ const. in Eq. (2), $n \approx$ const. is obtained. This is why n in the upstream diverging magnetic field region seems to be almost independent of B and S as shown in Fig. 2 (b).

As is done in Ref [19], the right hand side of the following equation is also investigated;

$$(1 - M^2)\frac{dM}{ds} = \frac{1 + M^2}{nc_s}S + \frac{M(1 + M^2)}{c_s}\frac{dc_s}{ds} + \frac{\tilde{c}_s^2}{c_s^2}\frac{M}{B}\frac{dB}{ds}. \tag{4}$$

This equation describes the parallel gradient of M in the steady state which is obtained by combining Eqs. (1) and (2). Here, $\tilde{c}_s \equiv \sqrt{(T_{i,\perp} + T_e)/m_i}$ is defined for convenience although $\tilde{c}_s^2/c_s^2 \approx 1$ holds due to the isotropy of T_i. Eq. (4) tells that the right hand side needs to change its sign from positive to negative at the sonic-transition point s_{trans} so that the plasma flow can continuously transfer from subsonic to supersonic. In Fig. 2 (f), a bifurcation of solutions concerning s_{trans} is observed; $s \sim 0.51$ m at which the effect of S becomes weak enough to balance with that of the diverging magnetic field in Eq. (4) and $s \sim 2.33$ m at which the effect of the contracting magnetic field becomes weak enough to balance with that of the sound-speed gradient term in Eq. (4). If the former became s_{trans}, the plasma would not satisfy the Bohm criterion due to the region of the contracting magnetic field. Thus, the plasma chooses the latter as s_{trans} in this case as shown in Fig. 2 (c). The plasma flow transfers from subsonic to supersonic due to the magnetic nozzle effect. The Mach number at the sheath entrance becomes $M_t \sim 2.13$. This tendency of M profile is similar to the experimental result of a linear device [14].

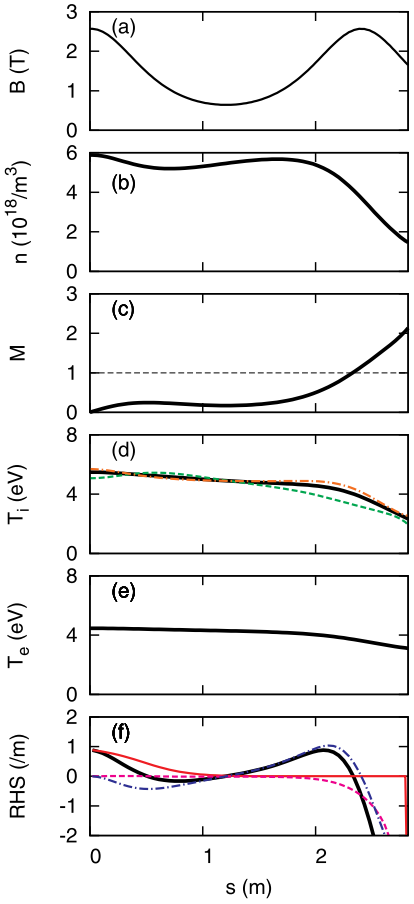

Fig. 2. Solution from the AIP model; (a) the magnetic field strength B, (b) plasma density n, (c) Mach number M, (d) effective isotropic ion temperature $T_i \equiv (T_{i,\parallel} + 2T_{i,\perp})/3$ (thick solid line) with parallel $T_{i,\parallel}$ (thin broken line) and perpendicular $T_{i,\perp}$ (thin chain line) components, (e) electron temperature T_e and (f) the right hand side of Eq. (4) (thick solid line) with the first, (thin solid line), the second (thin broken line) and the third (thin chain line) terms of it.

3.2. Comparison with an analytical solution

In this section, only are Eqs. (1) and (2) solved under a condition of $T_i = 0$ (i.e. the ions are monoenergetic) and $T_e = 5$ eV in order to compare the solution with an analytical one. The Mach number M profile numerically obtained from the AIP model is shown in Fig. 3. Here, B_0 is the magnetic field strength at $s = 0$ and 2.39 m (i.e. the local maximum of B). The ions are accelerated in the magnetic nozzle and a supersonic plasma flow is obtained with the sonic-transition point s_{trans} located at the local maximum of B (i.e. $\partial_s B = 0$).

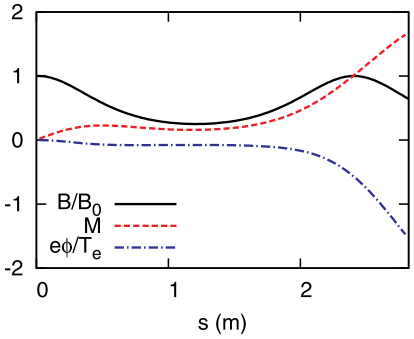

Fig. 3. Profiles of normalized magnetic field strength B/B_0 (solid line), Mach number M (broken line) and normalized electrostatic potential $e\phi/T_e$ (chain line) obtained from the AIP model.

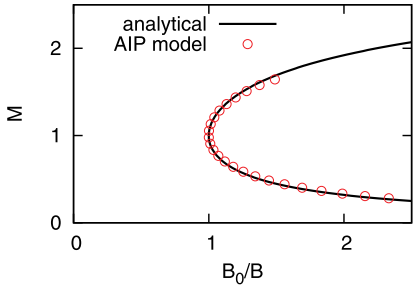

Fig. 4. Comparison between an analytical solution (solid line) and one from the AIP model (circles) of the Mach number M.

By combining the continuity of ions, $nV/B = \text{const.}$, the ion energy conservation, $m_i V^2/2 + e\phi = \text{const.}$ (ϕ represents the electrostatic potential), and the Boltzmann relation, $n \propto \exp(e\phi/T_e)$ [13], together with an assumption that s_{trans} is at the local maximum of B, the following analytical solution in a sourceless (i.e. $S = 0$) region is obtained;

$$\frac{B_0}{B} = \frac{1}{M}\exp\left(\frac{M^2 - 1}{2}\right). \tag{5}$$

The same analytical solution is also obtained by combining the steady state and sourceless version of Eqs. (1) and (2). Fig. 4 shows a direct comparison between the numerical solution in the $S \approx 0$ region and the analytical one, and a good agreement is obtained. The profile of the normalized electrostatic potential which is inversely calculated from the density profile and the Boltzmann relation is also shown in Fig. 3. It is found that the acceleration of the ions is caused by the ambipolar electric field in this case, which is not immediately clear from Eq. (2). In a finite-T_i case like Fig. 2, the effect of conservation of the magnetic moment also contributes to the acceleration of the plasma flow in the diverging-magnetic-field region. As a future work, this effect of conservation of the magnetic moment in high-T_i plasmas will be studied.

3.3. Comparison with B2 solutions

The solution from the AIP model shown in Fig. 2 is compared with that from the B2 code. Because the equation of parallel plasma momentum, Eq. (3), is parabolic, it requires an explicit boundary condition of the plasma flow velocity at a sheath entrance V_t. In this study, three kinds of boundary conditions of V_t are examined; (I) $V_t = c_s$ (i.e. the lower limit of the Bohm criterion), (II) V_t set to be the value obtained from the AIP model (i.e. $V_t = V_{t,AIP} \approx 3.31 \times 10^4$ m/s) and (III) V_t set to be the doubled AIP value (i.e. $V_t = 2V_{t,AIP} \approx 6.63 \times 10^4$ m/s).

Fig. 5 shows a direct comparison of solutions between the AIP model and the B2 code. Note that the B2 code uses a staggered grid in which V is evaluated at cell boundaries while the AIP model uses a collocated one and that the parallel grid width (≈ 46 mm) is fine enough to capture the spatial variation of every physical quantity. The profiles of the AIP model and the B2 code with three kinds of boundary conditions agree well with each other in the $M < 1$ region. As for the $M > 1$ region, on the other hand, it is demonstrated that unrealistic plasma flow profiles can be generated in principle depending on the boundary conditions for V_t although it is possible to adjust the profiles to those from the AIP model to some degree by choosing an appropriate V_t. That may lead to an overestimation or underestimation of A&M processes in realistic situations. It is also worth noting that the agreement of profiles between the AIP model and the B2 code in the $M < 1$ region is limited to high-collisionality conditions and that qualitative differences appear in low-collisionality conditions even though a viscous flux limit model is activated [24].

3.4. Effects of additional particle sources or sinks

Effects of particle sources or sinks in front of the target plate on the

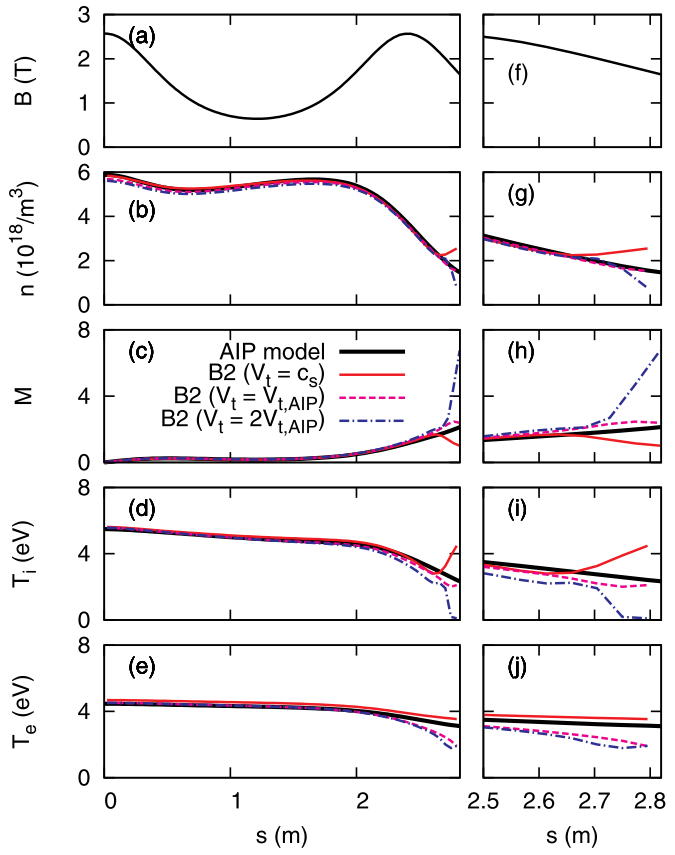

Fig. 5. Comparison of solutions from the AIP model (thick solid lines) and the B2 code (thin lines) with different boundary conditions of the plasma flow velocity at the sheath entrance V_t; (I) $V_t = c_s$ (thin solid lines), (II) V_t set to be the value obtained from the AIP model (i.e. $V_t = V_{t,AIP} \approx 3.31 \times 10^4$ m/s) (thin broken lines) and (III) V_t set to be the doubled AIP value (i.e. $V_t = 2V_{t,AIP} \approx 6.63 \times 10^4$ m/s) (thin chain lines). Figures (a)-(e) show the magnetic field strength B, the plasma density n, the Mach number M, the ion temperature T_i and the electron temperature T_e, respectively. Figures (f)-(j) show enlarged views of (a)–(e).

plasma flow profile are investigated by adding exponential-shape particle sources or sinks in front of the target plate which simply simulate A&M processes given as follows;

$$S = S_{add} \exp\left(\frac{s - L}{\lambda_{add}}\right). \quad (6)$$

Here, S_{add} is chosen from $-0.3S_0 \le S_{add} \le 3S_0$ and λ_{add} is fixed at 0.3 m for simplicity. For convenience, the flux amplification R defined as the particle flux at the target normalized by that without additional source or sink (i.e. $S_{add} = 0$) is introduced.

Typical solutions are shown in Fig. 6. As S_{add} becomes larger, s_{trans} moves toward the target plate leading to smaller M_t as shown in Fig. 6 (c) because the effect of the diverging magnetic field in front of the target is more relaxed in Eq. (4) as shown in Fig. 6 (f). If $S_{add} < 0$ is introduced, on the other hand, s_{trans} moves away from the target plate leading to larger M_t as shown in Fig. 6 (c) because the effect of the diverging magnetic field in front of the target is more enhanced in Eq. (4) as shown in Fig. 6 (f). It is hence indicated that a high recycling regime accompanied by a strong particle source region in front of the target may bring about subsonic flows and that plasma detachment regime accompanied by a strong particle sink region in front of the target may lead to supersonic flows. Fig. 7 summarizes M_t as a function of R. The reason why $M_t(R)$ is concave up as shown in Fig. 7 is that the coefficient of S in Eq. (4), i.e. $(1 + M^2)/(nc_s)$, decreases as R becomes large due to the increase in n and decrease in M as shown in Fig. 6 (b) and (c).

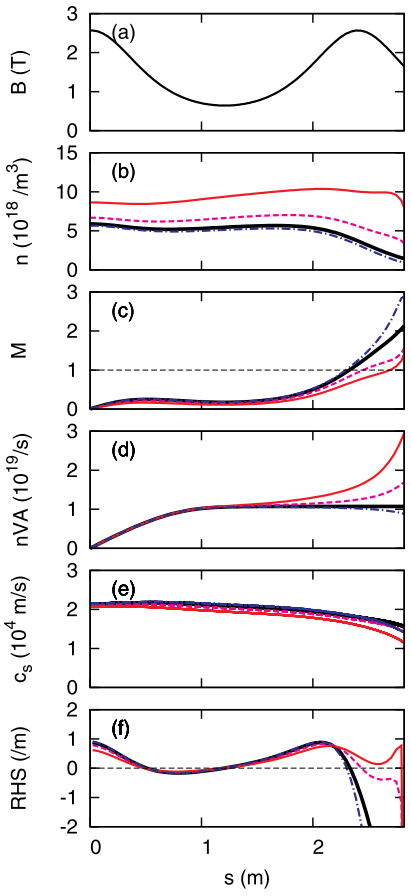

Fig. 6. Profiles of (a) B, (b) n, (c) M, (d) the area-integrated particle flux nVA, (e) c_s and (f) the right hand side of Eq. (4) for $S_{add} = 0$ (thick solid lines, $R = 1$), $3S_0$ (thin solid lines, $R \sim 2.75$), S_0 (thin broken lines, $R \sim 1.58$), $-0.3S_0$ (thin chain lines, $R \sim 0.83$).

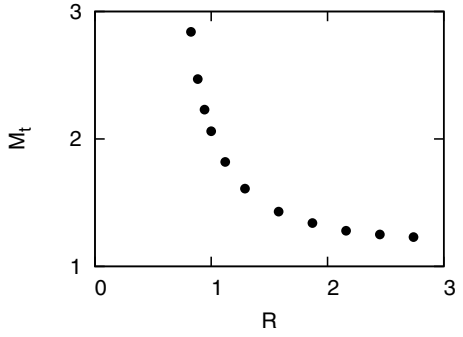

Fig. 7. Mach number at the sheath entrance M_t as a function of the flux amplification R.

3.5. Effects of the target position

The target position L_t is changed in a range of $L/2 \le L_t \le L$ in order to investigate effects of the downstream B profile on the upstream plasma flow profile. Fig. 8 shows typical solutions and the sonic-transition point s_{trans} is summarized as a function of L_t in Fig. 9. Because the temperature is roughly determined by $Q/S \propto T_{in}$ in this case, the c_s profile scarcely changes with L_t as shown in Fig. 8 (d). When the target is located between the original position of $s_{trans} \sim 2.33$ m and L, the information of the change in L_t does not propagate upstream and s_{trans} is almost fixed due to the choking of the plasma flow. If the target is in the range of ~ 1.7 m $< L_t < 2.33$ m, s_{trans} moves with L_t and, thus, the upstream M profile and corresponding n profile are affected as shown in

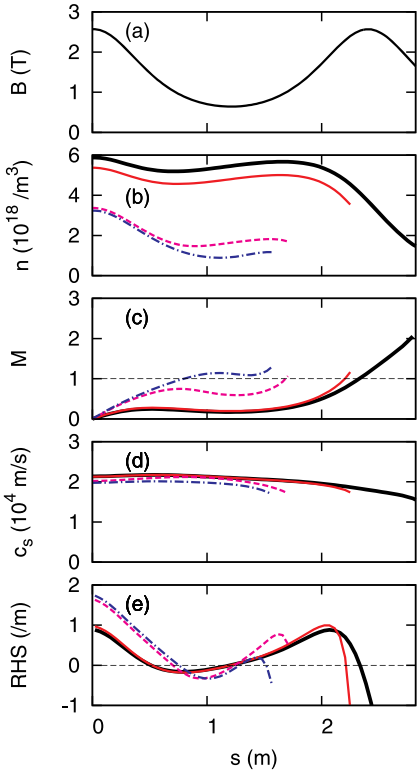

Fig. 8. Profiles of (a) B, (b) n, (c) M, (d) c_s and (e) the right hand side of Eq. (4) for L_t= 2.82 m (thick solid lines), 2.27 m (thin solid lines), 1.73 m (thin broken lines) and 1.59 m (thin chain lines).

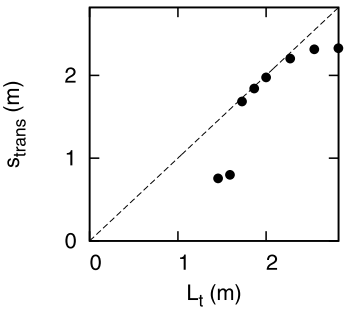

Fig. 9. Sonic-transition points s_{trans} as a function of the target position L_t.

Fig. 8 (b) and (c). When the target is set above $s \sim 1.7$ m, as shown in Fig. 9, s_{trans} jumps to the other branch discussed in Section 3.1, $s \sim 0.8$ m, because the effect of the downstream contracting magnetic field becomes weak enough as shown in Fig. 8 (e). Therefore, M profile and corresponding n profile are discontinuously changed as shown in Fig. 8 (b) and (c). Such a discontinuous change in s_{trans} and corresponding M profile caused by the bifurcating characteristics of s_{trans} can also be brought about by A&M processes because of the equivalence of S and dB/ds in Eq. (4).

4. Summary and future works

An SXD is expected to resolve the issue of rigorous particle and heat loads onto the divertor plates by its total flux expansion. Because of its magnetic-nozzle structure, a self-consistent treatment of supersonic plasma flows can be important in theoretical and numerical studies on the performance of an SXD. The AIP model enables to treat supersonic plasma flows self-consistently by describing the parallel plasma momentum transport with a hyperbolic equation keeping the finite effect of the parallel viscosity. In this study, plasma flow patterns in an SXD-like configuration are investigated by using the AIP model.

As a numerical solution from the AIP model, a collisional plasma is generated and hence the ion temperature is almost isotropic. A supersonic plasma flow is obtained due to the magnetic nozzle effect. The profile of the right hand side of the equation of the parallel gradient of the Mach number, Eq. (4), shows that the sonic-transition point has bifurcation characteristics and that a plasma chooses a proper branch to satisfy the Bohm criterion. Another numerical solution from the AIP model is compared with an analytical one in a case of monoenergetic ions and isothermal electrons and a good agreement is obtained. It also indicates that the acceleration of ions is caused by the ambipolar electric field in this case. Comparison with the Braginskii's plasma fluid model (the B2 code) is also conducted. In the subsonic plasma flow region, the profiles from the AIP model and the B2 code are almost identical due to high collisionality of the plasma. In the supersonic plasma flow region, on the other hand, various unphysical profiles are created by the B2 code depending on the boundary conditions of the plasma flow at the sheath entrance which might lead to an overestimation or underestimation of A&M processes. From a study of effects of additional particle sources or sinks in front of the target, it is found that a particle source/sink in front of the target brings about generations of subsonic/supersonic plasma flow profiles and that $M_t(R)$ becomes concave up. In order to investigate effects of the downstream B profile on the upstream plasma flow profile, the target position is changed. It is found that a discontinuous change in the sonic-transition point and corresponding profile of plasma flow can happen due to the bifurcating characteristics of the sonic-transition point. Such a phenomenon can also be brought about by A&M processes.

In the present paper, an SXD-like configuration is used which is much shorter and simpler compared to realistic SOL-divertor regions of existing or future torus devices. By using this SXD-like configuration, we intended to make the computational time short and to efficiently obtain physical insights on supersonic plasma flows generated by the magnetic nozzle effect. Also, we chose a high-collisionality plasma in this paper because plasma conditions which are more important in an engineering sense such as a high-recycling or a detached plasma are of high collisionality. As future works, simulations on SOL-divertor plasmas of a fusion device incorporating an SXD is planned. Effects of A&M processes on the plasma flow in an SXD will be studied by introducing some neutral models. In addition, effects of supersonic plasma flows on impurity transport and radiation efficiency will be studied.

Acknowledgments

This work is partly supported by the IEA Technology Collaboration Programme on the Development and Research on Plasma Wall Interaction Facilities for Fusion Reactors (PWI TCP) and the NINS program of Promoting Research by Networking among Institutions (Grant Number 01411702).

References

[1] P.M. Valanju, et al., Phys. Plasmas 16 (2009) 056110.
[2] D.D. Ryutov, Phys. Plasmas 14 (2007) 064502.
[3] H. Reimerdes, et al., Nucl. Fusion 57 (2017) 126007.
[4] C. Theiler, et al., Nucl. Fusion 57 (2017) 072008.
[5] T. Takimoto, et al., Fusion Eng. Des. 124 (2017) 235–238.
[6] D. Moulton, et al., Plasma Phys. Controlled Fusion 59 (2017) 065011.
[7] M.V. Umansky, et al., Nucl. Mater. Eng. 12 (2017) 918–923.
[8] E. Havlíčková, et al., Plasma Phys. Controlled Fusion 57 (2015) 115001.
[9] T.W. Petrie, et al., Nucl. Fusion 53 (2013) 113024.
[10] B. Lipschultz, F.I. Parra, I.H. Hutchinson, Nucl. Fusion 56 (2016) 056007.
[11] P.C. Stangeby, Modified 2 point model of the SOL to allow for variation in r_{target}, http://starfire.utias.utoronto.ca/divimp/publications/2PM-with-R_t-variation-10Aug11-inc.pdf.
[12] R.H. Cohen, D.D. Ryutov, Phys. Plasmas 6 (1999) 1995–2001.
[13] R.H. Cohen, D.D. Ryutov, Contrib. Plasma Phys. 44 (2004) 111–125.
[14] M. Inutake, et al., Arxiv:physics/0410205[physics.plasm-ph].

[15] M. Inutake, et al., J. Plasma Fusion Res. 78 (2002) 1352–1360.
[16] S.I. Braginskii, Rev. Plasma Phys. 1 (1965) 205. Consultants Bureau, New York
[17] O. Marchuk, M.Z. Tokar, J. Comput. Phys. 227 (2007) 1597–1607.
[18] L. Isoardi, et al., J. Comput. Phys. 229 (2010) 2220–2235.
[19] R. Goswami, et al., Phys. Plasmas 21 (2014) 072510.
[20] S. Togo, et al., J. Nucl. Mater. 463 (2015) 502–505.
[21] S. Togo, et al., J. Comput. Phys. 310 (2016) 109–126.
[22] S. Togo, et al., Contrib. Plasma Phys. 56 (2016) 729–735.
[23] S. Togo, et al., Contrib. Plasma Phys. 58 (2018) 556–562.
[24] S. Togo, et al., Plasma Fusion Res. 13 (2018) 3403022.
[25] B.J. Braams, NET, Report no. 68, (1987). (EUR-FU/XII-80/87/68)